doi:10.15625/2525-2518/21266



Synthesis of single phase brookite tio₂ nanomaterials from different titanium complexes in application of methyl orange degradation and hydrogen evolution reaction

Vu Viet Thang^{1, 2}, Norbert Steinfeldt², Ta Hong Duc^{1, *}

¹School of Chemical Engineering, Hanoi University of Science and Technology, 1 Dai Co Viet, Hai Ba Trung, Ha Noi, Viet Nam.

*Emails: duc.tahong@hust.edu.vn

Received: 2 August 2024; Accepted for publication: 16 October 2025

Abstract. This research focus on preparation of brookite TiO₂ materials from two different precursor as titanium glycolate and titanium lactate complexes. The single phase of brookite TiO₂ is synthesized successfully by hydrothermal process and confirmed by the X-ray diffraction (XRD) results. The scanning electron microscope (SEM) analysis shows that the nanorod and cubic-like morphology of brookite TiO₂ material are obtained by applying the titanium glycolate and lactate complex, respectively. The synthesized conditions are also investigated by changing the type and the amount of OH sources. All the single phase brookite TiO₂ samples are determined to contain a small amount of oxygen vacancies, which can by proved by the UV – Vis Diffuse reflectance spectroscopy (UV-Vis DRS) and X-ray photoelectron spectroscopy (XPS) measurement. The photoactivities of as-prepared brookite catalysts are tested in the application of methyl orange (MO) degradation and the hydrogen evolution reaction (HER), showing that the prepared cubic-like nanoparticle brookite sample Ti-NP-U9 exhibits higher activities compared with nanorod brookite TiO₂ and even the commercial TiO₂ P25. These results showing that the activity of brookite TiO₂ is highly depended on the morphology and promising for further study to enhance the photocatalytic performance.

Keywords: TiO₂; brookite; nanorods brookite; cubic-like nanoparticles brookite; photocatalytic degradation; hydrogen evolution reaction

Classification numbers: 2.4.2, 3.4.2

1. INTRODUCTION

Among many kinds of semiconductors, titanium dioxide (TiO_2) has proven to be an outstanding material as a promising photocatalyst, with numerous advantages like abundance, nontoxic nature, and photochemical stability [1 - 3]. Generally, TiO_2 exists mainly in three crystalline polymorphs as anatase, rutile, and brookite [4, 5]. While rutile is the stable phase, anatase and brookite are metastable and, brookite TiO_2 are readily transformed to rutile when heated at high temperature [6,

²Leibniz-Institut für Katalyse e.V. (LIKAT), Albert-Einstein-Str. 29a, 18059 Rostock, Germany

7]. During the sol-gel method, TiO_2 is normally formed in anatase phase, whereas brookite is often observed as a by-product of the precipitation. TiO_2 materials contain single phase of brookite without anatase or rutile is difficult to synthesize, therefore, photocatalytic activity research of this polymorph is still limited.

Brookite TiO₂ powder was firstly synthesized in the late 1950s by using titanium (IV) compounds during hydrothermal processes. A mixture of anatase and brookite could be obtained by thermal treatment of the amorphous TiO₂ powder [8]. Keesmann et al. synthesized pure brookite by hydrolysis of titanium tetraisopropoxide to obtain amorphous TiO2, following by hydrothermal reaction [9]. Many studies indicate that the formation of single phase brookite highly depends on the synthesis conditions and are difficult to control [10,11]. To inhibit the contamination of other phases, Kominami et al. prepared microcrystalline brookite by solvothermal reaction of oxobis(2,4pentanedionato-O,O') titanium (TiO(acac)₂) with ethylene glycol at 300 °C [12]. Until now, many inorganic and organic precursors have been employed to prepare brookite powder, such as TiCl₄ [13, 14], Ti(SO₄)₂ [15,16], titanium tetraisopropoxide [17], titanium butoxide [18], etc. Numerous studies indicate that water-soluble titanium complexes remain stable for years as neutral pH aqueous solutions, without precipitate formation, unlike traditional titanium sources like titanium chloride, titanium sulfate, and titanium alkoxide, which readily hydrolyze in the presence of moisture [19,20,21]. Additionally, these water-soluble titanium complexes are stable across a broad pH spectrum, from highly acidic (<1) to alkaline (approx. 14), even at room temperature. As a result, they can be easily managed and utilized under diverse synthesis conditions. The ligands in these complexes are readily available organic acids, such as glycolic and citric acids, making the use of these titanium compounds in the production of titanium-based materials potentially more costeffective and less harmful in terms of by-products. Therefore, these water-soluble titanium complexes are considered more environmentally friendly than traditional titanium agents.

In terms of photocatalytic activity, the phase component of TiO_2 materials is one of main factors significantly influencing to the performance, due to directly concerning to electronic properties (bandgap, photoinduced electron – hole separation, trapping sites) [22]. While the photoactivities of anatase and rutile TiO_2 have been widely investigated, brookite TiO_2 is still poorly researched due to difficulty in synthesis. Nevertheless, density functional theory calculations have exhibited that the exposed facet (210) of brookite is more efficiency in photocatalytic application comparing to the common surface (101) of anatase [23]. Li et al. researched different polymorphs of TiO_2 and proved that nanoplates brookite showed higher activity for the bleaching of methyl orange under UV light [24]. Brookite TiO_2 also was found to be more efficient in the application of photocatalytic degradation of Rhodamine B [25, 26].

Herein, in this work, the titanium glycolate and titanium lactate complexes have been selected to synthesize pure phase brookite TiO_2 materials during hydrothermal reactions. The phase structure, morphologies, and characteristics of as-prepared materials were analyzed by listed methods. The photocatalytic activities of all samples were investigated by the photocatalytic degradation of methyl orange and the photo-hydrogen evolution reaction under simulated solar light and white light irradiation, respectively. Noteworthily, the performance of cubic-like nanoparticle brookite TiO_2 showed higher activity comparing to nanorod material and even commercial P25.

2. EXPERIMENTAL SECTION

2.1. Chemicals

Metallic titanium powder (-325 mesh, 99.99 %) and urea (NH_2CONH_2 , 99 ÷ 100.5 %) were purchased from Alfa Aesar. Aqueous ammoniac (NH_3 , 25 %) and hydrogen peroxide (H_2O_2 , 30

%) were obtained from Labochem and VWR Chemical BDH, respectively. Glycolic acid ($C_2H_4O_3$, 99 %) and titanium (IV) chloride (TiCl₄, for synthesis) were purchased from Sigma Aldrich. Sodium lactate ($C_3H_5NaO_3$, 60 % in water) was purchased from TCI. Triethanolamine ($C_6H_{15}NO_3$, 98 %) and methyl orange ($C_{14}H_{14}N_3NaO_3S$, 99 %) were obtained from Sigma Aldrich and Acros Organics, respectively. Aeroxide TiO₂ P25 was used as catalyst reference and purchased from Evonik Degussa.

2.2. Materials preparation

2.2.1. Synthesis of nanorods brookite TiO₂

In a typical synthesis, titanium powder (478 mg, 10 mmol) was reacted with aqueous NH_3 (11.2 mL, 25 %) and H_2O_2 (40 mL, 30 %) in a 100 mL conical flask at 4–5 °C overnight to form a yellowish transparent solution. Subsequently, glycolic acid (27 mmol) was added, and the mixture was stirred at 50 °C for 30 min. The solution was then heated to 90 °C to remove water and excess H_2O_2 , affording a solid yellow titanium complex.

$$Ti + 3 H_2O_2 + NH_3 \rightarrow [Ti(OH)_3O_2]^- + 2 H_2O + NH_4^+$$
 (1)

$$4 \left[\text{Ti}(OH)_{3}O_{3} \right]^{2} + 6 C_{2}H_{4}O_{3} + 2 H_{2}O \Rightarrow \left[\text{Ti}_{4}(C_{3}H_{2}O_{3})_{4}(C_{5}H_{5}O_{3})_{5}(O_{7})_{4}O_{7} \right]^{6} + 10 H_{2}O + 2 H_{3}O^{+}$$
 (2)

For the next step, the obtained titanium complex (10 mmol) was completely dissolved in 20 mL of distilled water. A certain amount (approx. 10.7 mL) of the complex solution and 10 mL of NH $_3$ solution (25 %) were transferred into a 45 mL Teflon-lined stainless-steel autoclave. The hydrothermal reaction was performed at 180 °C for 24 hours. When finished, the produced solid materials were centrifuged and washed with distilled water at least 5 times. Finally, the white powders were dried overnight at 80 °C and denoted as Ti-NR-N. For comparison, 10 mL of NH $_3$ solution was altered by 10 mL of aqueous solution contained 1; 1.5; and 2 g of urea, respectively, in the hydrothermal process. The final products were denoted as Ti-NR-Ux, where x was the amount of employed urea during synthesis process.

2.2.2. Synthesis of nanoparticles brookite TiO₂

$$TiCl_4 + 6 H_2O \rightarrow [Ti(OH)_2(OH_2)_4]^{2+} + 2 H^+ + 4 Cl^-$$
 (3)

$$[\text{Ti}(OH)_2(OH_2)_4]^{2+} + 3 C_3H_4O_3^{2-} \rightarrow [\text{Ti}(C_3H_4O_3)_3]^{2-} + 2 OH^- + 4 H_2O$$
 (4)

Briefly, 1.65 mL of titanium (IV) chloride was added dropwise into a 100 mL conical flask contained 60 mL of distilled water, which was cooled by an ice-water bath. After 30 minutes of stirring, an acidic solution that contains a water-soluble titanium complex was formed (Equation 3). Subsequently, a certain amount of urea (3; 5; 7; and 9 g, respectively) was added and dissolved in the solution with continuous stirring. Then, 5 mL of sodium lactate liquor was dropped in the mixture and stirred for more 30 minutes to form the titanium lactate complex (Equation 4). All the prepared solution was transferred into a 125-mL Teflon autoclave and the reaction was carried out at 200 °C in 12 hours. The final crystallization products were separated by centrifugation, washed at least 5 times with water, dried at 80 °C overnight, and denoted as Ti-NPx (where x is the amount of urea using in the hydrothermal process).

2.3. Material characterization

The X-ray diffraction patterns were measured with an X'pert Pro diffractometer (Panalytical, Almelo, the Netherlands) using a scanning rate of 0.05o/s and monochromatized Cu Ka radiation.

The SEM micrographs were recorded using a Merlin VP compact device (Zeiss, Oberkochen, Germany).

The BET surface areas and porosities of the samples were obtained by N_2 adsorption at 196 °C using a Micromeritics ASAP 2020 (USA) instrument and calculated by the Brunauer-Emmett – Teller (BET) and Barrett- Joyner-Halenda (BJH) methods, respectively. Prior the analysis, the samples were degassed at 200 °C for 10 hours.

The light absorption was determined by UV-Vis Diffuse reflectance spectroscopy (UV-Vis DRS) with a Carry-5000 (Agilent, USA) spectrophotometer from 200 to 800 nm with $BaSO_4$ as the reference.

The XPS (X-ray Photoelectron Spectroscopy) measurements were performed on an ESCALAB 220iXL (Thermo Fisher Scientific) with monochromated Al K α radiation (E = 1486.6 eV). Samples are prepared on a stainless-steel holder with conductive double-sided adhesive carbon tape. The measurements are performed with charge compensation using a flood electron system combining low energy electrons and Ar+ ions (pAr = 1×10-7 mbar). The electron binding energies are referenced to the C 1s core level of carbon at 284.8 eV (C-C and C-H bonds). For quantitative analysis, the peaks were deconvoluted with Gaussian-Lorentzian curves using the software Unifit 2023. The peak areas were normalized by the transmission function of the spectrometer and the element specific sensitivity factor of Scofield.

2.4. Investigation of photocatalytic activities

2.4.1. Photocatalytic degradation reaction

The photocatalytic activity of the as-prepared materials was evaluated by degrading methyl orange (MO) under artificial sunlight (white light). Typically, 30 mg of brookite TiO₂ catalyst were dispersed in 60 mL of MO solution (30 mg/L) in a photocatalytic reactor (Figure S1). Before illumination, adsorption–desorption equilibrium was established by stirring in the dark for 30 min. The reactor was irradiated in a SUNTEST CPS+ system (ATLAS) simulating sunlight (λ = 290–800 nm, 80,000 Lux) (Figure S2) for 3 h. During irradiation, 1 mL aliquots were withdrawn at intervals, filtered, and analyzed by HPLC (Agilent 1260) with a Phenomenex C18 column (Kinetex, 2.6 µm, 150 × 3 mm). The mobile phase was acetonitrile (0.05 vol% TFA)/water (0.15 vol% TFA) = 80:20 v/v, flow rate 0.6 mL·min⁻¹, column temperature 40 °C, and injection volume 12 µL. UV detection was performed at 500 nm. TOC contents of initial and final solutions were measured using a TOC analyzer (Multi-N/C 3100, Analytik Jena).

2.4.2. Photocatalytic hydrogen evolution reaction

Photocatalytic hydrogen evolution reaction (HER) was carried out in a 100 mL double jacket cylindrical glass reactor (Figure S3). The reaction temperature was kept at 25 °C by flowing water through the outer wall of the reactor. A 300 W Xenon lamp (LSE341, LOT-QuantumDesign) equipped with a 90 ° deflection reflector system (MS 90) containing a dichroic mirror was applied as the light source (Figure S4). Typically, 25 mg of catalyst, 45 mL of distilled water, and 5 mL of triethanolamine (TEOA) were added into the photo-reactor. Subsequently, the obtained suspension was homogenized in an ultrasonic bath for 15 min. Afterwards, the photoreactor was installed into the testing system and the suspension was purged with Argon at a high flow rate (approx. 130 mL/min) to remove the oxygen content in the suspension and in the system lines for 30 minutes followed by reducing the Argon flow rate to 2.5 mL/min and kept in the photocatalytic process as carrier gas. The gas content and the formed hydrogen was detected online every 15 minutes by gas chromatography (GC, Agilent 6890) using a thermal conductivity detector (TCD). After purging

the photo-reactor with Argon, the measurement by GC was performed to ensure the amount of oxygen inside the system was very low before switching on the lamp. The reaction was carried out in 5 hours of white light irradiation.

The amount of H₂ produced per time (hydrogen production rate) was quantized using the following equation:

$$R_{H2} = \frac{F_{Ar} \times A_{H2} \times 60000}{V_m \times f_{H2} \times 100 vol\%} \quad (\mu \text{mol·h}^{-1})$$

where: F_{Ar} is the Argon flowrate (mL·min⁻¹); A_{H2} is the area of the hydrogen peak detected by GC; V_m is the molar volume at 25 °C ($V_m = 24.5 \text{ mL·mmol}^{-1}$); and f_{H2} is the calibration factor of hydrogen (was determined as vol%). The amount of formed hydrogen with time (µmol) was calculated by integrating the R_{H2} value over different reaction duration.

3. RESULTS AND DISCUSSION

3.1. Structure and Morphology

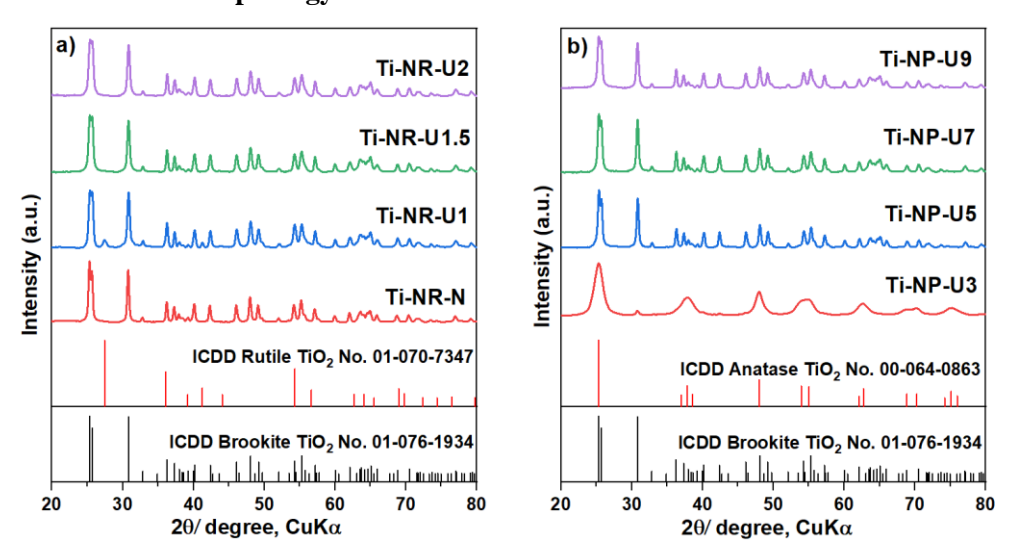


Figure 1. The XRD patterns of the TiO₂ materials synthesized from a) titanium glycolate complex and b) titanium lactate complex.

The X-ray diffraction patterns (Figure 1a, b) demonstrate the successfully synthesis of the brookite TiO_2 materials, with the presence of the (211) characteristic peak at $2\theta = 30.83^{\circ}$ (ICDD No.01-076-1934) [18,27]. According to Figure 1a, the Ti-NR-N samples contain highly pure brookite phase, in the absence of anatase characteristic peak at $2\theta = 62.57^{\circ}$, when synthesized from titanium-glycolate complex with NH₃ aqueous solution during the hydrothermal processes [28]. In the hydrothermal conditions, urea is commonly utilized to supply a consistent source of hydroxide anions via its decomposition, generates the OH anion in the reaction solution, thus providing a basic environment conducive to the formation of brookite TiO_2 , as indicated by the chemical reaction below [29,30]:

$$NH_2(CO)NH_2 + 3H_2O \rightarrow 2NH_4 \cdot OH + CO_2$$

The small diffraction peak observed at position of $2\theta = 27.44$ ° obtained when using 1 g of urea can readily be explained by the (110) plane of rutile TiO₂, indicating a mixture of brookite/rutile

phases in the Ti-NR-U1 sample [31,32]. If the amount of urea was increased to 1.5 g and above, pure brookite phase could be formed when using the titanium glycolate complex. The pH value of final solution is also measured after the hydrothermal process, and in range from 9 to 10 when synthesis with NH₃ solution or with 1.5 g and 2 g urea, respectively. Figure 1b also illustrates high quality brookite TiO₂ synthesized by using titanium lactate as precursor during the hydrothermal process. When the amount of urea introduced was too low, the material has poor crystallization ability of anatase phase and consists of a small amount of brookite (the Ti-NP-U3 sample). When the highest amount of urea was employed, the pH value of final solution was detected as approx. 9. It could be seen from Figure 1b that, single phase of brookite TiO₂ can be only formed at high pH value when employing the titanium lactate complex during hydrothermal process, corresponding to the XRD patterns of Ti-NP-U5, Ti-NP-U7, and Ti-NP-U9 sample.

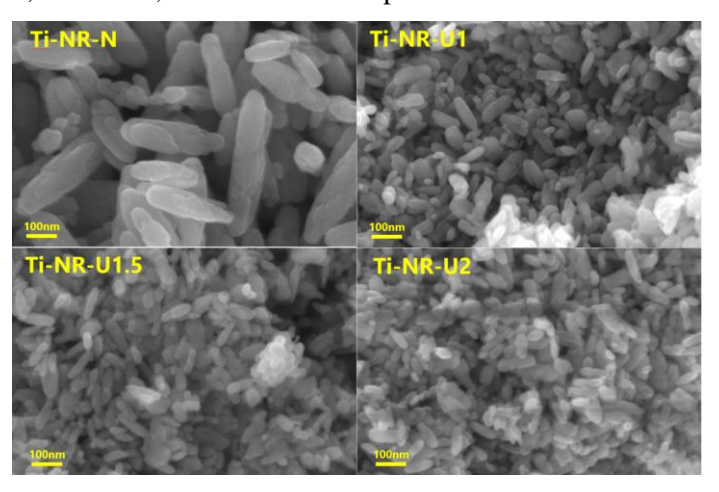


Figure 2. SEM images of nanorods brookite TiO₂ synthesized from titanium glycolate complex

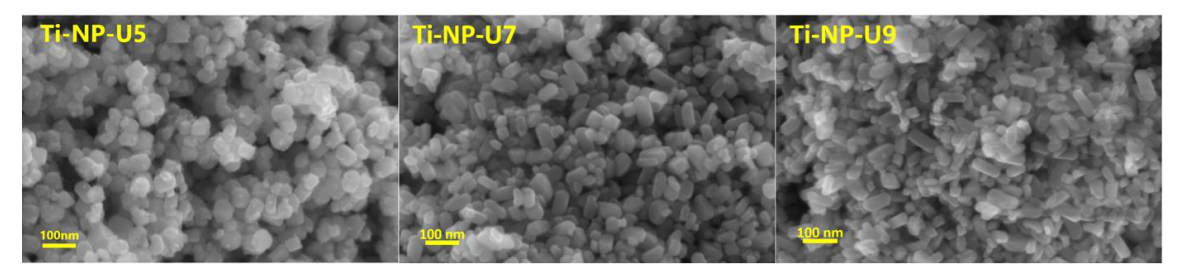


Figure 3. SEM images of nanoparticles brookite TiO₂ synthesized from titanium lactate complex

The morphology of the formed brookite phase is affected by the Ti-precursor used. According to Figure 2, the brookite TiO₂ materials synthesized by titanium glycolate complex obtain the nanorods morphology (Ti-NR-N, Ti-NR-U1, Ti-NR-U1.5, and Ti-NR-U2 samples, respectively). The size of the nanorods depends on the base sources employed during the hydrothermal processes. When using the NH₃ solution to adjust the pH value of the hydrothermal process, the TiO₂ nanorods have a diameter up to 80 nm and a length up to 250 nm. Meanwhile, when using urea instead of NH₃ solution, the nanorods are smaller and the rods are more uniform. The diameter of the rods decreases to approx. 20 nm and its length to about 70 nm. When the brookite TiO₂ was prepared from titanium lactate complex, the morphology has been changed, as shown in Figure 3. When using 5g of urea, cubic nanoparticles are formed with a particle diameter of approximately 30 to 40 nm (Ti-NP-U5 material). Increased urea amount during synthesis process leads to TiO₂ crystals consist of ununiform truncated tetragonal

shape nanoparticles, which had the length up to ≈ 90 nm, the width up to 50 nm, and a thickness up to 20 nm (Ti-NP-U7 and Ti-NP-U9 samples, respectively).

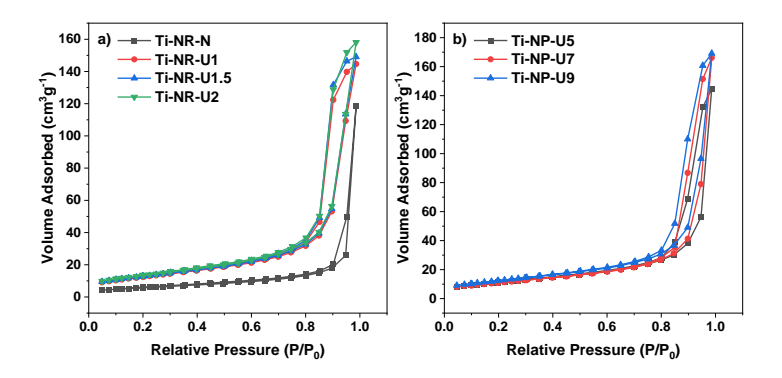


Figure 4. The N₂ adsorption – desorption isotherms of brookite TiO₂ synthesized from: a) titanium glycolate complex and b) titanium lactate complex.

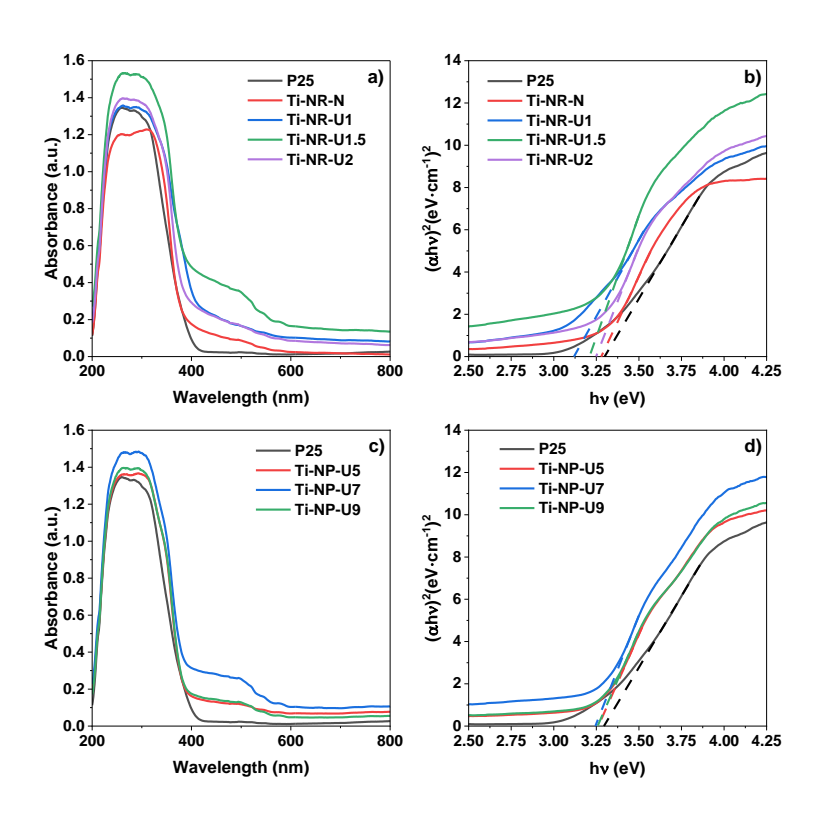


Figure 5. (a) UV-Vis DRS and (b) Tauc plot of nanorod brookite TiO₂; (c) UV-Vis DRS and (d) Tauc plot of nanoparticle brookite TiO₂

The specific surface area of TiO_2 catalyst is a critical influence factor to the photoactivities [33 - 35]. The BET measurement of all different brookite TiO_2 materials are summarized in Table 1. When synthesized from titanium glycolate complex, the specific surface area of the material doubled when replacing the base source from NH_3 aqueous solution to urea. This result is in relevant to the

significant change of the particle parameters obtained by SEM images. Continuing to increase the amount of urea during synthesis slightly increases the specific surface area of the final material. Besides, this value of brookite TiO_2 material witnessed slight changes when employed different amounts of urea during the hydrothermal process when using the titanium lactate complex. The N_2 adsorption – desorption isotherms of all materials include hysteresis loops (Figure 4). The isotherms could be assigned to IV type for similar mesoporous materials, according to IUPAC classification [36, 37].

The UV-Vis DRS results of as-synthesized nanorods brookite TiO₂ samples are presented in Figure 5a, with Aeroxide P25 was measured as reference material. Strong absorption in the ultraviolet region (below 420 nm) is observed from all TiO₂ samples. However, comparing to P25, nanorods samples exhibit light absorption in the wavelength of visible range. The sample Ti-NR-U1.5 exhibits higher light absorption than the others. This behavior can be attributed to the formation of oxygen vacancies (OVs) inside the TiO₂ lattice during synthesis processes [38,39]. Due to the Tauc plot (Figure 5b), the bandgap energies are calculated to be 3.28, 3.12, 3.2, and 3.25 eV corresponding to Ti-NR-N, Ti-NR-U1, Ti-NR-U1.5, and Ti-NR-U2 material, respectively. The XRD analysis indicates that the Ti-NR-U1 material comprises two TiO₂ phases as brookite and a minor quantity of rutile. Rutile possesses an indirect bandgap, approximately 3.0 eV, whereas brookite has a direct bandgap [40,41]. The synthesized materials' calculations are predicated on brookite's direct bandgap, suggesting that the presence of rutile's indirect bandgap, which is lower than brookite's, may have decreased the overall bandgap of the Ti-NR-U1 sample comparing to the others. The optical properties of nanoparticle materials show similarities with nanorods samples (Figure 5c), which indicate the possibility of OVs formation during the hydrothermal synthesis despite of using different titanium precursors. All samples show the absorbance capability in the visible light region. with the highest of Ti-NP-U7 sample. In Figure 5d, the bandgap energy of Ti-NP-U5, Ti-NP-U7, and Ti-NP-U9 are estimated as 3.26, 3.24, and 3.26 eV, respectively.

Materials	Surface area (m²·g-¹)	Pore radius (nm)	Total pore volume (cm ³ ·g ⁻¹)	Bandgap (eV)
Ti-NR-N	20.7	15.8	0.18	3.28
Ti-NR-U1	45.5	9.0	0.23	3.12
Ti-NR-U1.5	46.4	9.1	0.23	3.2
Ti-NR-U2	48.5	9.0	0.25	3.25
Ti-NP-U5	40.6	8.6	0.22	3.26
Ti-NP-U7	39.7	8.6	0.25	3.24
Ti-NP-U9	45.1	8.9	0.26	3.26

Table 1. BET surface area of the as-prepared TiO₂ samples.

XPS measurement was conducted to analyze the chemical states of the Ti-NR-N, Ti-NR-U1.5, and Ti-NP-U9 samples (Figure 6). The presence of Ti and O elements in as-synthesized samples are revealed by the survey spectrums (Figure 6a). The C element appeared in all cases is attributed to surface carbon from the XPS internal standard measurement. Figure 6b described the characteristic Ti 2p peak of all materials. With two nanorod samples, the Ti 2p peaks are located at 458.5 and approx. 464.1 eV, corresponding to Ti $2p_{3/2}$ and Ti $2p_{1/2}$, respectively [42]. When synthesized the nanoparticle material from titanium lactate complex, these peaks are slightly shifted to lower binding energy (458.3 eV and 464.0 eV for the Ti $2p_{3/2}$ and Ti $2p_{1/2}$, respectively). In Figure 6c, the largest O 1s peak of all samples relate to the Ti – O bond, while

the small peaks at approx. 530.8 eV could be associated with the surface absorbed oxygen [42,43]. Furthermore, all the brookite TiO₂ samples synthesized from titanium complexes possess a small characteristic O 1s peak at the position of 532.1 eV, 531.9 eV, and 531.8 eV of Ti-NR-N, Ti-NR-U1.5, and Ti-NP-U9, respectively, which can be ascribed to oxygen vacancies [44,45]. In conclusion, the obtained XPS results of Ti-NR-N, Ti-NR-U1.5, and Ti-NP-U9 sample, in agree with the UV-Vis DRS analysis, reveal the formation of oxygen vacancies during the synthesis of brookite TiO₂ materials by hydrothermal method employing titanium glycolate and lactate complexes.

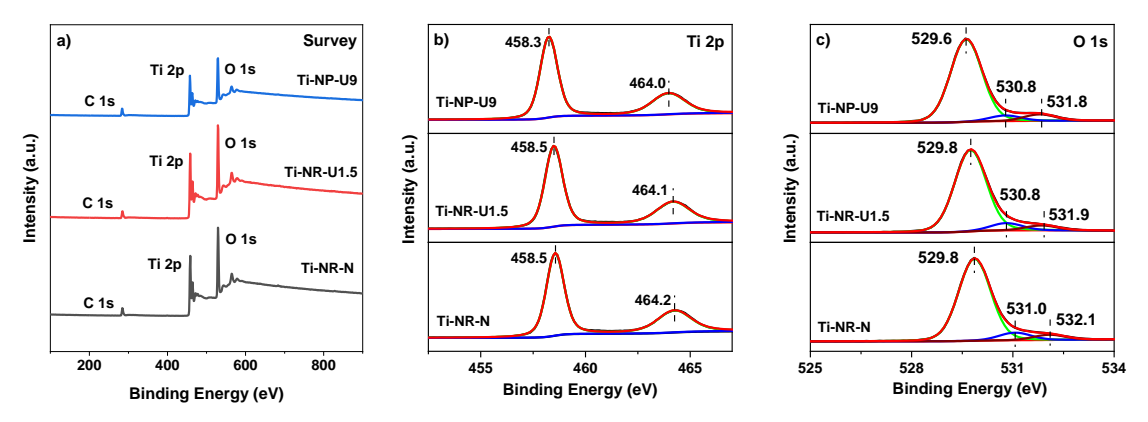


Figure 6. High – resolution XPS spectra of a) survey spectrum; b) Ti 2p peaks; and c) O 1s peaks of Ti-NR-N, Ti-NR-U1.5, and Ti-NP-U9 materials.

3.2. Photocatalytic activities

3.2.1. Photocatalytic degradation of methyl orange

Figure 7a describes the efficiency of photocatalytic degradation of methyl orange (MO) solution under simulated sunlight condition of brookite TiO₂ nanorods samples synthesized using different OH sources as NH₃ and urea. When using NH₃ aqueous solution in the synthesis process, the resulting Ti - NR - N catalyst exhibits the lowest activity with only circa 60 % of MO is decomposed after 3 hours. Meanwhile, when using urea as a base source for synthesis, the obtained catalysts show significantly higher activities and achieves the best treatment efficiency of 99 % of MO with sample Ti - NR - U1.5. However, in comparison with the commercial product as Aeroxide TiO₂ P25, the activities of as-prepared nanorods catalysts are still remarkably lower. The brookite TiO₂ nanorods sample with the highest activity has a reaction rate constant k of 0.023 min⁻¹, lower than that of P25 with the k value reaching 0.033 min⁻¹ (Figure 7b). The above analysis results are also consistent with the TOC measurement results of the final solution, showing the ability of P25 to decompose organic substances into CO₂ and water very strongly during the reaction with the remaining organic carbon content only reached 3.1 %. Meanwhile, the nanorods Ti-NR-U1.5 sample with the best activity still had 20 % organic residue left (Figure 7c).

Figure 7d shows the photocatalytic degradation activities of cubic-like nanoparticle brookite TiO₂ catalysts synthesized using different amounts of urea. Ti-NP-U3 material shows the lowest activity and not being able to degrade MO completely after 3 hours of irradiation. This can be explained by the XRD result, showing that Ti-NP-U3 contains restricted crystallinity TiO₂, which may exhibit the photocatalytic activity of the catalyst [46,47]. However, the materials synthesized with higher amount of urea inhibit very high photocatalytic activities and completely decompose MO after 3 hours of solar irradiation. Furthermore, Ti-NP-U7 and Ti-NP-U9 catalysts reveal superior MO

conversion ability compared to the commercial P25. Figure 7e shows that the reaction rate constant k of the two samples Ti-NP-U7 and Ti-NP-U9 reached 0.036 and 0.042 min⁻¹, respectively, higher than the value of 0.033 min⁻¹ of P25. Figure 7f shows that the both TOC values of Ti-NP-U9 and P25 are similar, only 3.1% remains after reaction.

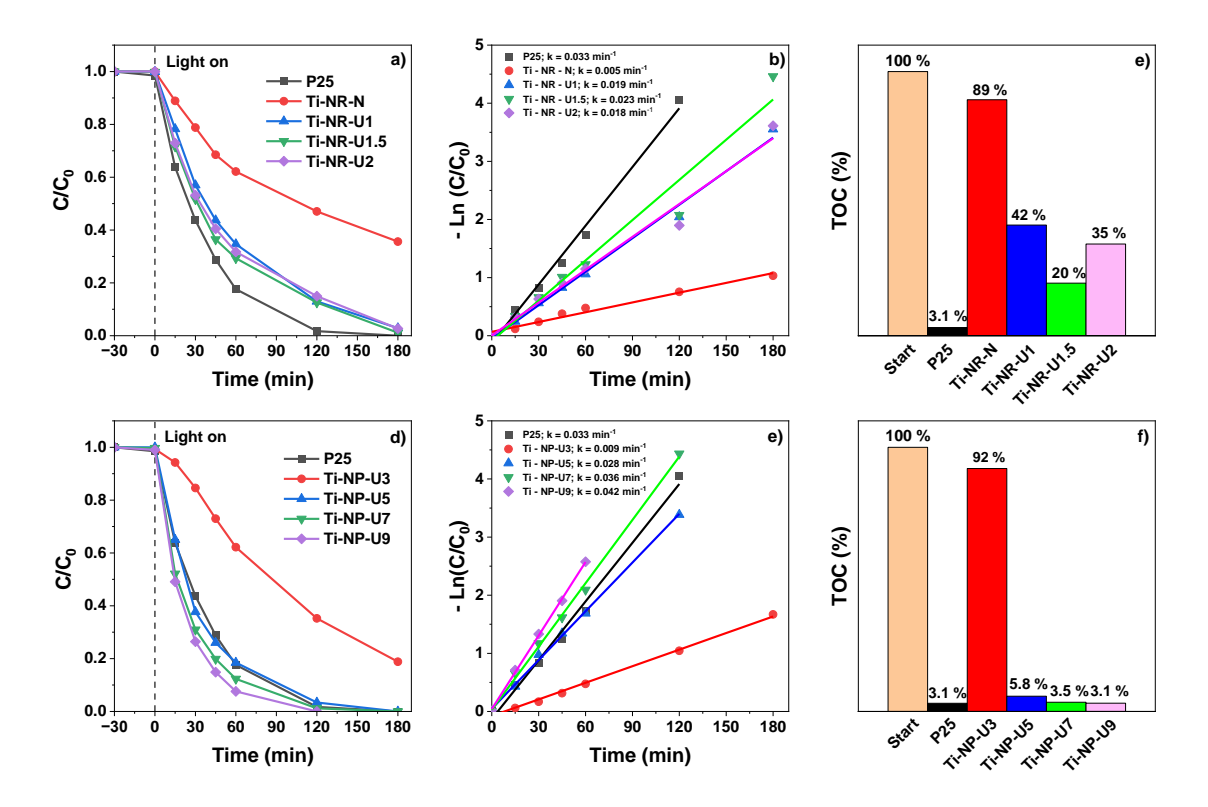


Figure 7. The photocatalytic degradation of methylorange under solar light by different TiO₂ materials (a, b); the pseudo-first-order kinetics fitted curves of reactions (c, d); and the TOC removal comparison (e, f).

3.2.2. Photocatalytic hydrogen evolution reaction

Several studies indicated that the photocatalytic hydrogen evolution from anatase/brookite composites and pure brookite surpasses that of pure anatase TiO2, and even commercial P25 under UV/visible light irradiation [48,49]. Therefore, two brookite TiO₂ samples as nanorods Ti-NR-U1.5 and cubic-like nanoparticles Ti-NP-U9, which exhibited best MO photodegradation activities, were chosen to evaluate their activities in the photocatalytic hydrogen evolution reaction using TEOA as a sacrificial agent under white light irradiation. Figure 8a shows the amount of hydrogen produced profile under 5 hours of white light irradiation. In the photodecomposition reaction, brookite nanorods Ti-NR-U1.5 material has significantly lower activity than P25. However, in the hydrogen generation application, the amount of hydrogen produced by two material samples are almost equivalent. For the brookite cubic-like nanoparticles Ti-NP-U9 sample synthesized from titanium lactate complex, the photochemical hydrogen generation activity is clearly superior comparing to P25 and the brookite nanorods sample synthesized from titanium glycolate complex. The hydrogen evolution rate over reaction time was estimated (Figure S5) and Figure 8b illustrates that the average hydrogen generation rate of P25, Ti-NR-U1.5, and Ti-NP-U9 is 240.5, 232.2, and 317.9 μmol·h⁻¹·g⁻¹, respectively. The photo-HER results prove that the brookite TiO₂ synthesized from titanium glycolate and lactate complexes have outstanding potential in this application, even in comparison

with the commercial product P25. Furthermore, the different activities in the HER reaction of the two nanorods and cubic-like nanoparticles samples showed that the photocatalytic activities of pure phase brookite TiO₂ materials strongly depends on their morphology and exposed-facets, which is consistent with some previously published reports on the influence of facet-controlled brookite TiO₂ on their photocatalytic activity. [50, 51]

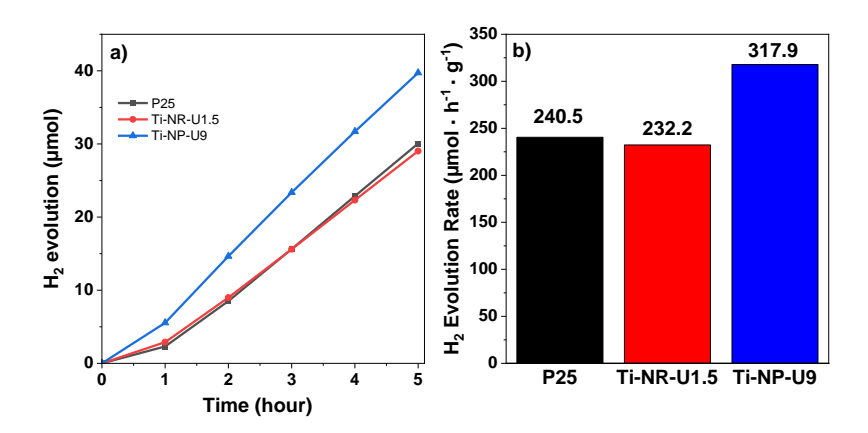


Figure 8. a) Hydrogen generation profile and b) the average hydrogen evolution rate of different brookite TiO₂ in comparison with P25.

4. CONCLUSIONS

The single phase brookite TiO2 have been synthesized successfully from two different titanium complexes by the hydrothermal method. The nanorods brookite TiO₂ can be obtained by using titanium glycolate complex, meanwhile, the formation of cubic-like nanoparticle morphology is occurred with the precursor as titanium lactate complex. The synthesized conditions were also investigated when adjusted the OH sources during hydrothermal processes by using NH₃ aqueous solution or different amount of urea. All as-prepared brookite TiO₂ materials contain a low amount of oxygen vacancies, confirmed by the UV-Vis DRS and XPS analysis results. The photocatalytic activities of all synthesized catalysts are evaluated in the application of methyl orange degradation, with the reaction rate constant of nanorod Ti-NR-U1.5 and cubic-like nanoparticle Ti-NP-U9 materials were 0.023 min⁻¹ and 0.042 min⁻¹, respectively, incomparison with 0.033 min⁻¹ of commercial P25. Furthermore, in the HER tests, the average hydrogen evolution rates of P25, Ti-NR-U1.5, and Ti-NP-U9 samples were 240.5, 232.2, and 317.9 µmol·h⁻¹·g⁻¹, respectively. The results indicate that single-phase brookite TiO2 is highly promising for photocatalytic degradation and hydrogen evolution reactions. Moreover, the asprepared cubic-like nanoparticle brookite demonstrating higher photocatalytic activity than the nanorod brookite sample suggests that the overall performance of brookite TiO2 materials is significantly influenced by their morphologies and exposed facets.

Acknowledgements. The financial support provided by the German Academic Exchange Service (DAAD) and the project RoHan was gratefully acknowledged.

Credit authorship contribution statement. Vu Viet Thang: Experimentation, Writing – original draft; Norbert Steinfeldt: Supervision, Writing – review editing; Ta Hong Duc: Supervision, Writing – review editing.

Declaration of competing interest. The authors declare that they have no known competing financial interests or personal relationships that could have appeared to influence the work reported in this paper.

REFERENCES

- Jenny Schneider, Masaya Matsuoka, Masato Takeuchi, Jinlong Zhang, Yu Horiuchi, Masakazu Anpo, Detlef W. Bahnemann - Understanding TiO₂ Photocatalysis: Mechanisms and Materials. Chemical Reviews, 114(19) (2014) 9919-9986 https://doi.org/10.1021/cr5001892
- Yusnita Sari, Paulus Lobo Gareso, Bidayatul Armynah, Dahlang Tahir A review of TiO₂ photocatalyst for organic degradation and sustainable hydrogen energy production. International Journal of Hydrogen Energy, 15 (2024) 984-996 https://doi.org/10.1016/j.ijhydene.2023.11.126
- 3. Wail Al Zoubi, Abbas Ali Salih Al-Hamdani, Baek Sunghun, Young Gun Ko A review on TiO₂-based composites for superior photocatalytic activity. Reviews in Inorganic Chemistry, **41**(4) (2021) 213-222 https://doi.org/10.1515/revic-2020-0025
- Eddy DR, Permana MD, Sakti LK, Sheha GAN, Solihudin, Hidayat S, Takei T, Kumada N, Rahayu I. - Heterophase Polymorph of TiO₂ (Anatase, Rutile, Brookite, TiO₂ (B)) for Efficient Photocatalyst: Fabrication and Activity. Nanomaterials, 13(4) (2023) 704 https://doi.org/10.3390/nano13040704
- 5. Maolin Zhang, Tiedan Chenb, Yunjian Wang Insights into TiO₂ polymorphs: highly selective synthesis, phase transition, and their polymorph-dependent properties. RSC Advances, **7** (2017) 52755-52761 https://doi.org/10.1039/C7RA11515F
- 6. Tarek A. Kandiel, Lars Robben, Ayad Alkaima, Detlef Bahnemann Brookite versus anatase TiO₂ photocatalysts: phase transformations and photocatalytic activities. Photochemical & Photobiological Sciences, **12** (2013) 602–609 https://doi.org/10.1039/c2pp25217a
- 7. Miao Song, Zexi Lu, Dongsheng Li Phase transformations among TiO₂ polymorphs. Nanoscale, **12** (2020) 23183-23190 https://doi.org/10.1039/D0NR06226J
- 8. Bach, H. Zur Bildung von Brookit in dünnen TiO₂-Schichten. Naturwissenschaften **51** (1964) 10–11 https://doi.org/10.1007/BF00601717
- 9. I. Keesmann Zur hydrothermalen Synthese von Brookit. ZAAC **346**(1-2) (1966) 30-43 https://doi.org/10.1002/zaac.19663460105
- 10. T. Mitsuhashi, M. Watanabe Brookite formation from precipitates containing calcium ions. Mineralogical Journal, **9**(4) (1978) 236-240 https://doi.org/10.2465/minerj.9.236
- 11. Pascal Arnal, Robert J. P. Corriu, Dominique Leclercq, P. Hubert Mutin, André Vioux Preparation of anatase, brookite and rutile at low temperature by non-hydrolytic sol-gel methods. Journal of Materials Chemistry, **6** (1996) 1925-1932 https://doi.org/10.1039/JM9960601925
- 12. Hiroshi Kominami, Masaaki Kohnoa, Yoshiya Kera Synthesis of brookite-type titanium oxide nano-crystals in organic media. Journal of Materials Chemistry, **10** (2000) 1151-1156 https://doi.org/10.1039/A908528I
- 13. M Koelsch, S Cassaignon, J.F Guillemoles, J.P Jolivet Comparison of optical and electrochemical properties of anatase and brookite TiO₂ synthesized by the sol–gel method. Thin Solid Films, **403-404** (2002) 312-319 https://doi.org/10.1016/S0040-6090(01)01509-7
- 14. Agatino Di Paola, Giovanni Cufalo, Maurizio Addamo, Marianna Bellardita, Renzo Campostrini, Marco Ischia, Riccardo Ceccato, Leonardo Palmisano Photocatalytic activity of nanocrystalline TiO₂ (brookite, rutile and brookite-based) powders prepared by

- thermohydrolysis of $TiCl_4$ in aqueous chloride solutions. Colloids and Surfaces A: Physicochemical and Engineering Aspects, **317**(1-3) (2008) 366-376 https://doi.org/10.1016/j.colsurfa.2007.11.005
- 15. Qian Xu, Jing Zhang, Zhaochi Feng, Yi Ma, Xiang Wang, Can Li Surface Structural Transformation and the Phase Transition Kinetics of Brookite TiO₂. Chemistry An Asian Journal, **5**(10) (2010) 2129-2303 https://doi.org/10.1002/asia.201000249
- 16. W. Luo, S.F. Yang, Z.C. Wang, Y. Wang, R. Ahuja, B. Johansson, J. Liu, G.T. Zou Structural phase transitions in brookite-type TiO2 under high pressure. Solid State Communications, 133(1) (2005) 49-53 https://doi.org/10.1016/j.ssc.2004.09.049
- 17. Gerko Oskam, Felipe de Jesús Peet Poot Synthesis of ZnO and TiO₂ nanoparticles. Journal of Sol-Gel Science and Technology, **37** (2006) 157-160 https://doi.org/10.1007/s10971-005-6620-3
- 18. Bin Zhao, Feng Chen, Qiwei Huanga, Jinlong Zhang, Brookite TiO₂ nanoflowers. Chemical Communications, (2009) 5115-5117 https://doi.org/10.1039/B909883F
- 19. Makoto Kobayashi, Valery Petrykin, Koji Tomita, Masato Kakihana, Hydrothermal synthesis of brookite-type titanium dioxide with snowflake-like nanostructures using a water-soluble citratoperoxotitanate complex, Journal of Crystal Growth, **337**(1) (2011) 30-37 https://doi.org/10.1016/j.jcrysgro.2011.09.046
- 20. Tomita K, Petrykin V, Kobayashi M, Shiro M, Yoshimura M, Kakihana M. A water-soluble titanium complex for the selective synthesis of nanocrystalline brookite, rutile, and anatase by a hydrothermal method. Angew Chem Int Ed Engl. **45**(15) (2006) 2378-81 10.1002/anie.200503565
- 21. Kobayashi, M., Tomita, K., Petrykin, V. et al. Direct synthesis of brookite-type titanium oxide by hydrothermal method using water-soluble titanium complexes. J Mater Sci **43** (2008) 2158–2162 https://doi.org/10.1007/s10853-007-1912-3
- 22. S. Girish Kumar, K.S.R. Koteswara Rao, Comparison of modification strategies towards enhanced charge carrier separation and photocatalytic degradation activity of metal oxide semiconductors (TiO₂, WO₃ and ZnO). Applied Surface Science, **391**(Part B) (2017) 124-148 https://doi.org/10.1016/j.apsusc.2016.07.081
- 23. Wei-Kun Li, Xue-Qing Gong, Guanzhong Lu, Annabella Selloni, Different Reactivities of TiO₂ Polymorphs: Comparative DFT Calculations of Water and Formic Acid Adsorption at Anatase and Brookite TiO₂ Surfaces. The Journal of Physical Chemistry C, **112**(17) (2008) 6594-6596 https://doi.org/10.1021/jp802335h
- 24. Ji-Guang Li, Takamasa Ishigaki, Xudong Sun Anatase, Brookite, and Rutile Nanocrystals via Redox Reactions under Mild Hydrothermal Conditions: Phase-Selective Synthesis and Physicochemical Properties. The Journal of Physical Chemistry C, **111**(13) (2007) 4969-4976 https://doi.org/10.1021/jp0673258
- 25. Jimin Xie, Xiaomeng Lü, Jun Liu, Huoming Shu Brookite titania photocatalytic nanomaterials: Synthesis, properties, and applications. Pure and Applied Chemistry, **81**(12) (2009) 2407-2415 https://doi.org/10.1351/PAC-CON-08-11-12
- 26. Xiaojun Shen, Jinlong Zhang, Baozhu Tian, Masakazu Anpo Tartaric acid-assisted preparation and photocatalytic performance of titania nanoparticles with controllable phases of anatase and brookite. Journal of Materials Science, 47 (2012) 5743–5751 https://doi.org/10.1007/s10853-012-6465-4
- 27. Marianna Bellardita, Agatino Di Paola, Bartolomeo Megna, Leonardo Palmisano Absolute crystallinity and photocatalytic activity of brookite TiO₂ samples. Applied Catalysis B: Environmental, **201** (2017) 150-158 https://doi.org/10.1016/j.apcatb.2016.08.012

- 28. Wanbiao Hu, Liping Li, Guangshe Li, Changlin Tang, Lang Sun High-Quality Brookite TiO₂ Flowers: Synthesis, Characterization, and Dielectric Performance. Crystal Growth & Design, **9**(8) (2009) 3676-3682 https://doi.org/10.1021/cg9004032
- 29. Ángel Emilio García-Domínguez, Gilberto Torres-Torres, Juan Carlos Arévalo-Pérez, Adib Silahua-Pavón, Cecilia Sánchez-Trinidad, Srinivas Godavarthi, Reyna Ojeda-López, Uriel Alejandro Sierra-Gómez, Adrián Cervantes-Uribe, Urea assisted synthesis of TiO₂—CeO₂ composites for photocatalytic acetaminophen degradation via simplex-centroid mixture design, Results in Engineering, **14** (2022) 100443 https://doi.org/10.1016/j.rineng.2022.100443
- 30. X.Li, G.M.Kale, Urea-based hydrothermal synthesis of ITO nanopowders, Journal of Physics: Conference Series, **26** (2006) 319 10.1088/1742-6596/26/1/077
- 31. Guo Chen, Jin Chen, Zengkai Song, C. Srinivasakannan, Jinhui Peng A new highly efficient method for the synthesis of rutile TiO₂. Journal of Alloys and Compounds, **585** (2014) 75-77 https://doi.org/10.1016/j.jallcom.2013.09.056
- 32. I. M. Joni, L. Nulhakim, C. Panatarani Characteristics of TiO₂ particles prepared by simple solution method using TiCl₃ precursor. Journal of Physics: Conference Series, **1080** (2018) https://doi.org/10.1088/1742-6596/1080/1/012042
- 33. M. Hussain, R. Ceccarelli, D.L. Marchisio, D. Fino, N. Russo, F. Geobaldo Synthesis, characterization, and photocatalytic application of novel TiO₂ nanoparticles. Chemical Engineering Journal, **157**(1) (2010) 45-51 https://doi.org/10.1016/j.cej.2009.10.043
- 34. Obaid Ali Qamar, Farrukh Jamil, Murid Hussain, Sungjun Bae, Abrar Inayat, Noor S Shah, Ammara Waris, Parveen Akhter, Eilhann E. Kwon, Young-Kwon Park Advances in synthesis of TiO2 nanoparticles and their application to biodiesel production: A review. Chemical Engineering Journal, 460 (2023) 141734 https://doi.org/10.1016/j.cej.2023.141734
- 35. Samar Al Jitan, Giovanni Palmisano, Corrado Garlisi Synthesis and Surface Modification of TiO₂-Based Photocatalysts for the Conversion of CO₂. Catalysts, **10**(2) (2020) 227 https://doi.org/10.3390/catal10020227
- 36. Beata Michalkiewicz, Justyna Majewska, Grzegorz Kądziołka, Kamila Bubacz, Sylwia Mozia, Antoni W. Morawski Reduction of CO₂ by adsorption and reaction on surface of TiO₂-nitrogen modified photocatalyst. Journal of CO₂ Utilization, **5** (2014) 47-52 https://doi.org/10.1016/j.jcou.2013.12.004
- 37. S. Asuha, X.G. Zhou, S. Zhao Adsorption of methyl orange and Cr(VI) on mesoporous TiO2 prepared by hydrothermal method. Journal of Hazardous Materials, **181**(1-3) (2010) 204-210 https://doi.org/10.1016/j.jhazmat.2010.04.117
- 38. Xu Zhang, Min Cai, Naxin Cui, Guifa Chen, Guoyan Zou, Li Zhou Defective Black TiO₂: Effects of Annealing Atmospheres and Urea Addition on the Properties and Photocatalytic Activities. Nanomaterials, **11**(10) (2021) 2648 https://doi.org/10.3390/nano11102648
- 39. Muhammad Wajid Shah, Yunqing Zhu, Xiaoyun Fan, Jie Zhao, Yingxuan Li, Sumreen Asim & Chuanyi Wang Synthesis of Defective TiO_{2-x} Nanocrystals with High Surface Area and Tailoring Bandgap for Visible-light Photocatalysis. Scientific Reports **5** (2015) 15804 https://doi.org/10.1038/srep15804
- David O. Scanlon, Charles W. Dunnill, John Buckeridge, Stephen A. Shevlin, Andrew J. Logsdail, Scott M. Woodley, C. Richard A. Catlow, Michael. J. Powell, Robert G. Palgrave, Ivan P. Parkin, Graeme W. Watson, Thomas W. Keal, Paul Sherwood, Aron Walsh, Alexey A. Sokol, Band alignment of rutile and anatase TiO₂, Nature Materials, 12 (2013) 798–801 https://doi.org/10.1038/nmat3697

- 41. Akinobu Miyoshi, Shunta Nishioka, Kazuhiko Maeda, Water Splitting on Rutile TiO₂-Based Photocatalysts, Chemistry A European Journal, 24(69) (2018) 18204-18219 https://doi.org/10.1002/chem.201800799
- 42. Mohammed Ismael Enhanced photocatalytic hydrogen production and degradation of organic pollutants from Fe (III) doped TiO₂ nanoparticles. Journal of Environmental Chemical Engineering, **8**(2) (2020) 103676 https://doi.org/10.1016/j.jece.2020.103676
- 43. Dan Yan, Hui Miao, Jun Fan, Qiushuo Yu, Enzhou Liu, Tao Sun Constructing Dual Cocatalysts of Ni₂P–NiS-Decorated TiO₂ for Boosting Photocatalytic H₂ Evolution. Langmuir, **39**(46) (2023) 16648-16656 https://doi.org/10.1021/acs.langmuir.3c02719
- 44. Peng Kong, Hao Tan, Tingyu Lei, Jie Wang, Wenjun Yan, Ruiyi Wang, Eric R. Waclawik, Zhanfeng Zheng, Zhong Li Oxygen vacancies confined in conjugated polyimide for promoted visible-light photocatalytic oxidative coupling of amines. Applied Catalysis B: Environmental, 272 (2020) 118964 https://doi.org/10.1016/j.apcatb.2020.118964
- 45. Songmei Sun, Motonori Watanabe, Ji Wu, Qi An, Tatsumi Ishihara Ultrathin WO₃·0.33H₂O Nanotubes for CO₂ Photoreduction to Acetate with High Selectivity. Journal of the American Chemical Society, **140**(20) (2018) 6474-6482 https://doi.org/10.1021/jacs.8b03316
- 46. Marianna Bellardita, Agatino Di Paola, Bartolomeo Megna, Leonardo Palmisano Determination of the crystallinity of TiO₂ photocatalysts. Journal of Photochemistry and Photobiology A: Chemistry, **367** (2018) 312-320 https://doi.org/10.1016/j.jphotochem.2018.08.042
- 47. Agatino Di Paola, Marianna Bellardita, Leonardo Palmisano, Zuzana Barbieriková, Vlasta Brezová Influence of crystallinity and OH surface density on the photocatalytic activity of TiO₂ powders. Journal of Photochemistry and Photobiology A: Chemistry, **273** (2014) 59-67 https://doi.org/10.1016/j.jphotochem.2013.09.008
- 48. Kandiel, Tarek A. and Feldhoff, Armin and Robben, Lars and Dillert, Ralf and Bahnemann, Detlef W., Tailored Titanium Dioxide Nanomaterials: Anatase Nanoparticles and Brookite Nanorods as Highly Active Photocatalysts, Chemistry of Materials, **22**(6) (2010) 2050-2060 https://doi.org/10.1021/cm903472p
- 49. Burtrand I. Lee, Sujaree Kaewgun, Wooyul Kim, Wonyong Choi, Jae S. Lee, Eunsun Kim, Visible light photocatalytic properties of polymorphic brookite titania, Journal of Renewable and Sustainable Energy, 1 (2009) 023101 https://doi.org/10.1063/1.3096606
- 50. Gongbing Zhou, Ruidong Shi, Yanlu Dong, Crystal facet-controlled brookite TiO₂ nanostructures coupled with Ru nanoparticles for enhancing selective hydrogenation of benzene to cyclohexene, Chemical Engineering Journal, **484** (2024) 149635 https://doi.org/10.1016/j.cej.2024.149635
- 51. Ming Zhao, Hua Xu, Hungru Chen, Shuxin Ouyang, Naoto Umezawa, Defa Wang, Jinhua Ye, Photocatalytic reactivity of {121} and {211} facets of brookite TiO₂ crystals, Journal of Materials Chemistry A, **3** (2015) 2331-2337 https://doi.org/10.1039/C4TA06087C